Please cite this article as:
Tomasz Derda, Zbigniew Domański, Damage evolution on two-dimensional grids - comparison of load transfer rules, Scientific Research of the Institute of Mathematics and Computer Science, 2010, Volume 9, Issue 1, pages 5-15.
The website: http://www.amcm.pcz.pl/

DAMAGE EVOLUTION ON TWO-DIMENSIONAL GRIDS - COMPARISON OF LOAD TRANSFER RULES

Tomasz Derda, Zbigniew Domański

Institute of Mathematics, Czestochowa University of Technology, Poland
tomasz.derda@im.pcz.pl, zbigniew.domanski@im.pcz.pl

Abstract. The damage evolution occurring in a set of elements located in the nodes of the supporting two-dimensional grid is analysed within the stochastic approach. The element-strength-thresholds are drawn from a given probability distribution and the elements are treated as fibres within the Fibre Bundle Model. If an element fails, its load has to be transferred to the other intact elements. For different grid geometries we compare the evolution of the number of intact elements under the load with respect to three different load transfer rules: the global, the local and recently introduced so-called Voronoi load transfer rule. Our example system is an array of nanopillars.

Introduction

An evolving damage is an irreversible process causing the progressive destruction of the system components. The formation of fractures is initiated by the local microcracks, which grow when the local stress exceeds the threshold strength of the material. At some concentration, microcracks start to act coherently to enhance the local stress and induce more failures.

Knowledge of the fracture evolution up to the global rupture and its effective description is important for the analysis of the mechanical behaviour of the systems in response to the applied loads. From the theoretical point of view the understanding of the complexity of the rupture process has advanced due to the use of lattice models. An example of great importance is the family of transfer load mo dels, especially the Fibre Bundle Model (FBM) [1-5]. In the FBM a set of elements (fibres) is located in the nodes of the supporting lattice and the element-strength--thresholds are drawn from a given probability distribution. After an element has failed, its load has to be transferred to the other intact elements. Three different cases are considered: the global load sharing (GLS) - the load is equally shared by the remaining elements, the local load sharing (LLS) - only the neighbouring elements suffer from the increased load and the Voronoi load sharing (VLS) - the extra load is equally redistributed among the elements lying inside the Voronoi regions [6, 7] generated by a group of elements destroyed in subsequent intervals of time [8, 9].

Our paper is motivated by uniaxial tensile experiments on nanoscale materials that confirm substantial strength increase via the size reduction of the sample [10--13]. Especially studies on arrays of free-standing nanopillars subjected to uniaxial microcompression reveal the potential applicability of nanopillars as components for the fabrication of micro- and nano-electromechanical systems, micro-actuators or optoelectronic devices [10]. The aim of this contribution is to study the failure progress in an array of vertically oriented, and taper-free metallic nanoscale pillars subjected to an applied load. To illustrate the behaviour of the system, we map the array of nanopillars onto the surface with two-valued height function which correspond to intact and damaged pillars.

We apply the FBM to simulate failure by stepwise accumulation of the destructed pillars and we compute the number of time-steps elapsed until the array of pillars collapses. Numerical examples are presented to demonstrate the dynamic transformation of the rough surface evolving between two flat states: from all intact to all deformed pillars.

1. Mathematical model

Consider an array of N pillars located in the nodes of the supporting two dimensional lattice. The ensemble of pillars is subjected to an instantaneous longitudinal load F which is kept constant in time with a time step Δt considered here as a time scale. Under the work regime the pillars remain intact or some of them are damaged. Let $n_d(\tau)$ denote the number of pillars damaged at the time $t = \tau \cdot \Delta t$. The number $N_i(\tau)$ of intact pillars and the cumulative number $N_d(\tau) = n_d(1) + n_d(2) + \cdots + n_d(\tau - 1)$ of pillars damaged prior to τ evolve in time with the constraints: $N = N_i(\tau) + N_d(\tau)$, $N = N_i(0) = N_d(\infty)$ and $N_d(0) = 0$. To each pillar x_k we assign a critical load σ_k which is randomly distributed according to a distribution P_k. When the load $f_k(\tau)$ applied on a pillar x_k is bigger than σ_k, the pillar crashes. Any damage reduces $N_i(\tau)$ and causes a further increase of local loads.

1.1. The load transfer rules

Since the load value F applied at each time τ remains constant and N_i diminishes the load f locally felt by each pillar in subsequent time increases by an amount δf. This load increase is not uniform with respect to all the intact pillars, as it is assumed in the GLS version of the FBM, nor restricted to a nearest neighbourhood of the destroyed pillar in accordance with the LLS rule [2].

The VLS rule for the load-increase allocation is defined as follows [9]. A set of $N_i(\tau)$ pillars is split into $n_d(\tau-1)$ subsets grouping together pillars lying inside the Voronoi regions generated by $n_d(\tau-1)$ pillars destroyed in the time $\tau-1$. The load, previously carried by each of the damaged pillars is now equally distributed among the pillars belonging to the appropriate Voronoi region. More precisely, if ΔV_l, with k intact pillars, is the Voronoi region of the pillar destroyed at the site x_l then the load $f_l(\tau-1)$ is equally redistributed, with $\delta f(\tau) = f_l(\tau-1)/k$, among all the intact pillars inside the ΔV_l.

1.2. Two dimensional lattice geometries

As it was already mentioned we locate the pillars in the nodes of two dimensional lattices. In this work we analyse only regular arrangements, namely triangular, square and hexagonal symmetries shown in Figure 1. The lattice is represented by a set of nodes and edges connecting the pairs of neighbouring nodes. The distance between two nodes is defined as the number of edges contained in the shortest possible path between these nodes. Aforementioned lattices differ from each other in respect to so-called coordination number z of a node which is defined as the number of its nearest neighbours.

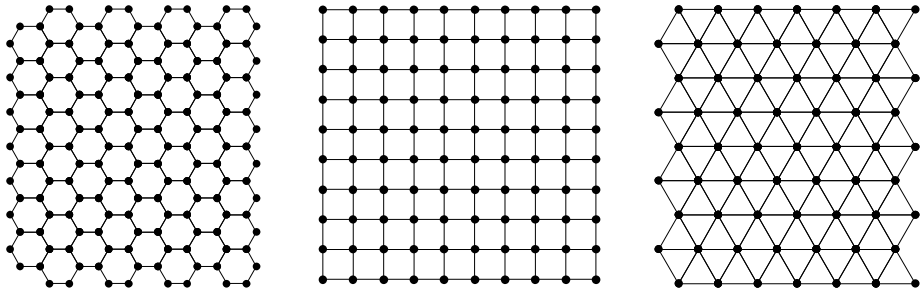

(a) (b) (c)

Fig. 1. Lattice geometries: a) hexagonal, b) square, c) triangular

1.3. The rough surface representation of the damage evolution

We map the array of nanopillars onto the lattice with two-valued height function $h_m(\tau)$:

$$h_m(\tau) = \begin{cases} 1 & \textit{if the node } m \textit{ is occupied by the intact pillar,} \\ 0 & \textit{otherwise} \end{cases} \tag{1}$$

Within this mapping the dynamics of the model can be seen as a rough surface evolving between two flat states: starting with an initially flat specimen we apply the load, thus the pillars start to be destroyed and after the last pillars fail the surface becomes flat. Figure 2 illustrates such surface for some time τ. Thus, the way the number $N_i(\tau)$ of intact pillars changes under the load can be characterised by the surface width [14, 15], defined as

$$W^2(\tau) = N^{-1} \sum_{1 \le m \le N} [h_m(\tau) - \langle h(\tau) \rangle]^2 \tag{2}$$

where $\langle h(\tau) \rangle$ is the average height over different sites at time τ.

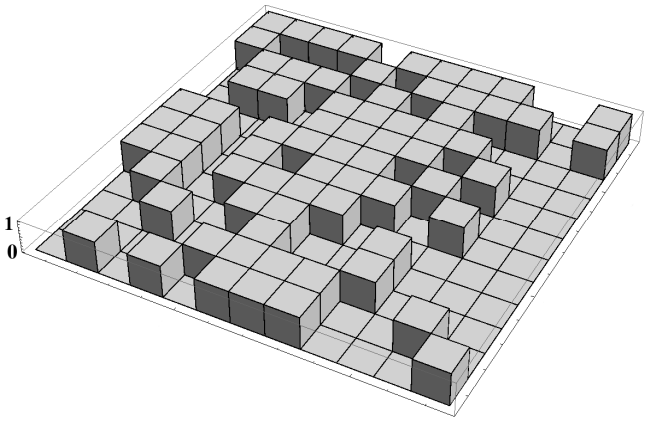

Fig. 2. An example of rough surface with two-valued height function defined by (1). Illustration for the set of nanopillars on the square lattice

2. Numerical modelling

We realised numerically the dynamic formation of the rough surface for two system sizes: $N \approx 2.5 \times 10^3$ and $N \approx 10^4$. Calculations have been done for three types of lattice, namely for hexagonal, square and triangular symmetries. In order to obtain accurate results simulations have been performed many times.

Average values of time steps of damaging process are shown in Table 1. As might be expected the geometry of lattice is irrelevant for the GLS scheme. In this case we obtained almost equal mean values of time steps of the damaging process for different lattice geometries. For the LLS scheme the damage process is the fastest for a triangular lattice and the slowest for a hexagonal lattice, so the greater number of neighbours the faster the damage process. Similarly to the GLS, for the VLS rule the damaging process lasts almost the same number of time steps irrespective of lattice geometry.

In general, as can be seen in Table 1, the damage process is the fastest for the GLS scheme and slowest for the LLS scheme. Thus, the VLS rule is intermediate form of load transfer between these extreme cases.

Table 1

The mean values of time steps of damaging process

System size	Lattice symmetry	Load transfer rules		
		GLS	VLS	LLS
$N \approx 2.5\times10^3$	hexagonal	12.086	16.528	18.480
	square	12.076	16.334	18.147
	triangular	12.022	16.551	16.584
$N \approx 10^4$	hexagonal	11.800	17.836	19.764
	square	11.787	17.516	19.296
	triangular	11.797	17.826	17.521

The parameters of the model introduced in Section 1 were the random critical loads σ_k with theirs probability distribution functions P_k, $k = 1,2,\ldots,N$, and the total load $F = f_0 \cdot N$. Here, $f_0 = f(\tau = 0)$ is the initial local load. In our simulations $f_0 = 1$. Since the pillars are mechanically independent we assume that σ_k are quenched random variables uniformly distributed on $[\sigma_0 - \Delta\sigma, \sigma_0 + \Delta\sigma]$, with $\sigma_0 = 1.65 \cdot f_0 = 1.65$ and $\Delta\sigma = 0.75 \cdot f_0 = 0.75$. We consider the following properties resulting from the VLS rule:

– evolution of the number of damaged pillars $n_d(\tau)$,

– the number of intact pillars per Voronoi region $\langle n_i(\tau)\rangle = \langle N_i(\tau)\rangle_V$.

These properties are distributed randomly and we are interested in how they vary in time. Next we investigate the statistical characteristics of $n_i(\tau)$ and $n_d(\tau)$. For this purpose we numerically construct distributions of these quantities for different lattice geometries as well as for different system sizes.

Figures 3 and 4 show the surface width $W^2(\tau)$ for the VLS and the LLS schemes, respectively. From Figure 3 we see that for the VLS rule geometry of lattice is irrelevant, because values of surface width are almost the same for different lattice types. For LLS scheme in the initial stages the values of $W^2(\tau)$ behaves similarly irrespective of lattice type. Since the value of $W^2(\tau)$ reaches maximum, the values of $W^2(\tau)$ for a triangular lattice start to vary from those obtained with the use of square and hexagonal ones.

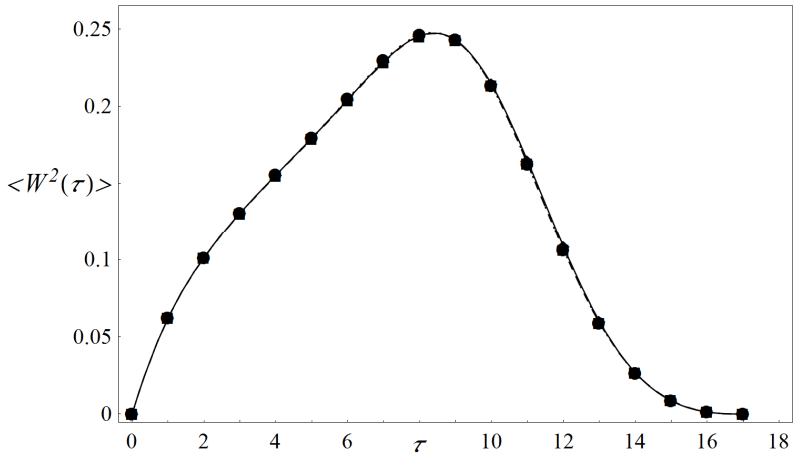

Fig. 3. The mode of surface width (2) vs. τ with the VLS rule for an array of 10^4 pillars. Comparison of lattice geometries: hexagonal (circle), square (square), triangular (diamond)

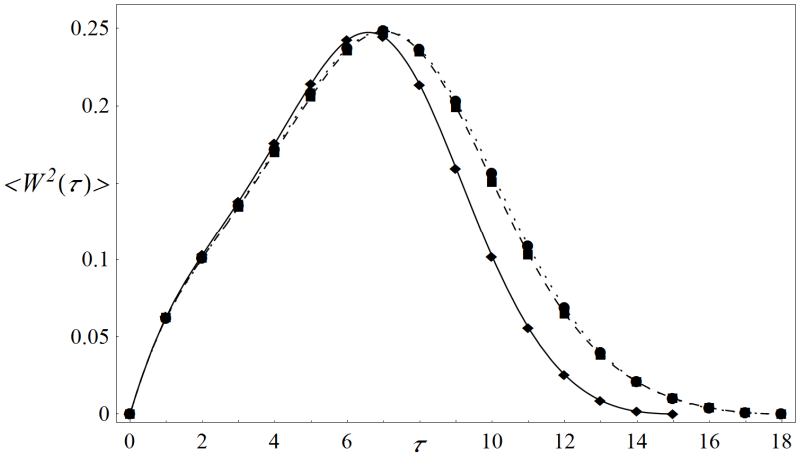

Fig. 4. The mode of surface width (2) vs. τ with the LLS rule for an array of 2.5×10^3 pillars. Comparison of lattice geometries: hexagonal (circle), square (square), triangular (diamond)

Figures 5 and 6 show the modes of the surface width $W^2(\tau)$ obtained within three different load transfer rules. From these Figures we see that almost half of the time the dominant value of $W^2(\tau)$ for the VLS rule lies between the lines corresponding to the GLS and the LLS rules. For the remaining time the behaviour of the VLS and the LLS is similar however the numerical values predicted by these rules differ.

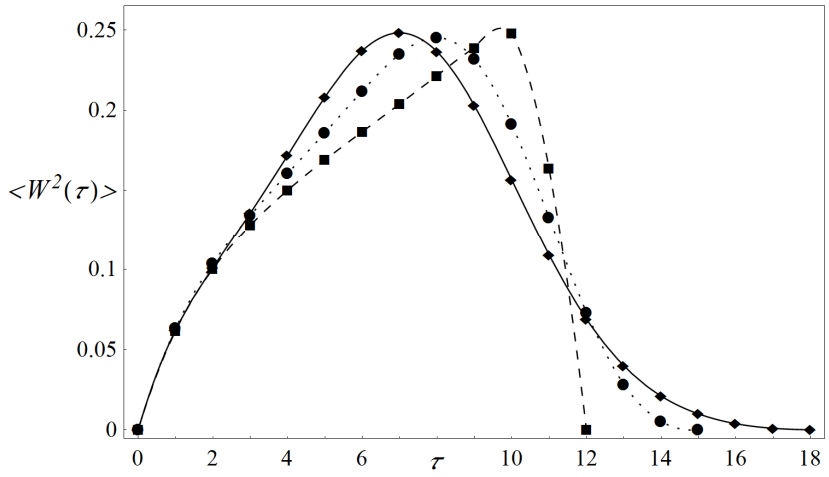

Fig. 5. The mode of surface width (2) vs. τ, for an array of 2.5×10^3 pillars on the hexagonal lattice. Comparison of load transfer rules: the GLS (square), the LLS (diamond) and the VLS (circle), the modes are taken from 10^3 samples for each rule

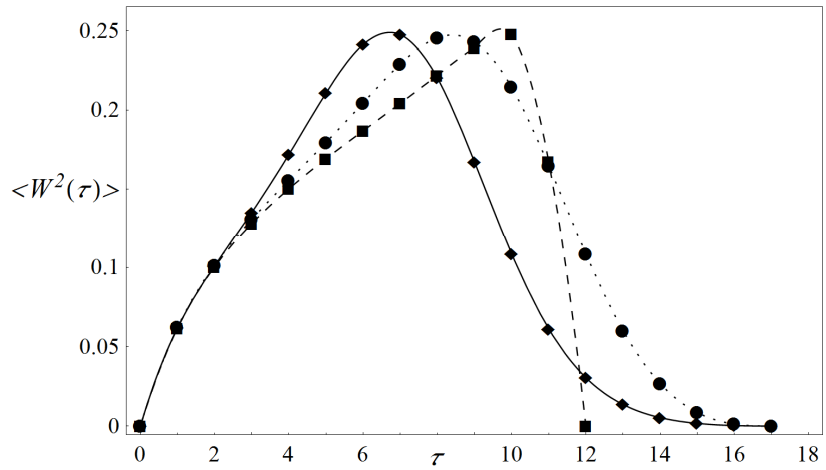

Fig. 6. The mode of surface width (2) vs. τ, for an array of 10^4 pillars on the triangular lattice. Comparison of load transfer rules: the GLS (square), the LLS (diamond) and the VLS (circle), the modes are taken from 10^3 samples for each rule

The quantities of main interest are: $n_d(\tau)$ (number of damaged pillars) and $\langle n_i(\tau)\rangle$ (number of intact pillars per Voronoi region).

Figures 7 and 8 illustrate the evolution of the mean value of $n_d(\tau)$ for the VLS and the LLS rules, respectively. In Figure 7 we compare the results obtained with the VLS rule for hexagonal, square and triangular lattices. Throughout the evolution the results obtained for aforementioned lattice geometries are very similar to each other. In the case of the LLS rule, as we can see in Figure 8, values of $n_d(\tau)$

for hexagonal and square lattices are similar to each other. For the triangular lattice in the middle stages the number of damaged pillars is greater in compare to the hexagonal and square ones. In the final stage of experiment $n_d(\tau)$ decreases rapidly for triangular lattice, while for the hexagonal and square ones this process is more smooth.

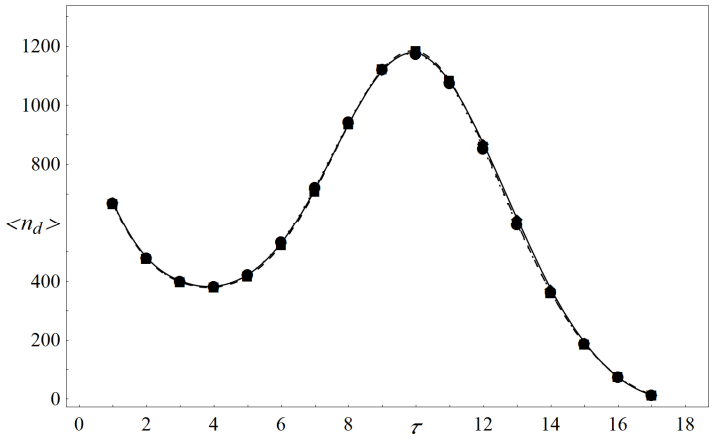

Fig. 7. Evolution of the average number of damaged elements $\langle n_d \rangle$ with the VLS rule. Comparison of lattices: hexagonal (circle), square (square), triangular (diamond). Here, $N \approx 10^4$ and the averages are taken over 10^3 samples

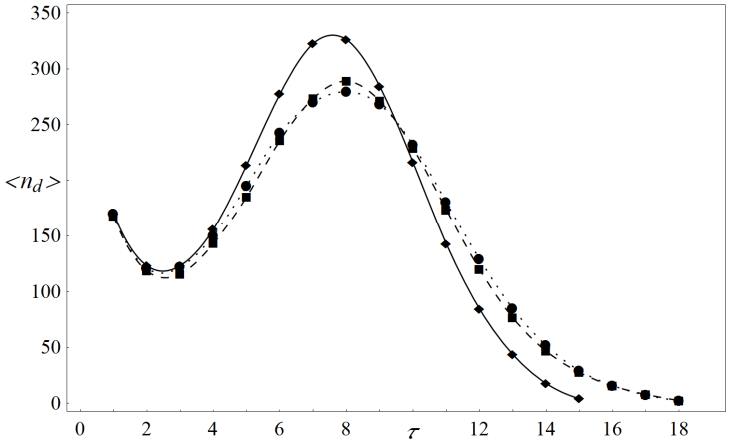

Fig. 8. Evolution of the average number of damaged elements $\langle n_d \rangle$ with the LLS rule. Comparison of lattices: hexagonal (circle), square (square), triangular (diamond). Here, $N \approx 2.5\times10^3$ and the averages are taken over 10^3 samples

In Figures 9 and 10 we show the evolution of the mean value of $n_d(\tau)$ for triangular and the hexagonal lattices. However these Figures present the difference of $\langle n_d \rangle$ for the GLS, the LLS and the VLS rules. In these cases throughout the evolu-

tion the results of VLS are closer to these of the LLS than to the result of the GLS. Within the GLS rule $n_d(\tau)$ grow rapidly before the system fails whereas both, the VLS and the LLS rules predict rather smooth extinction of the quantity of destroyed pillars.

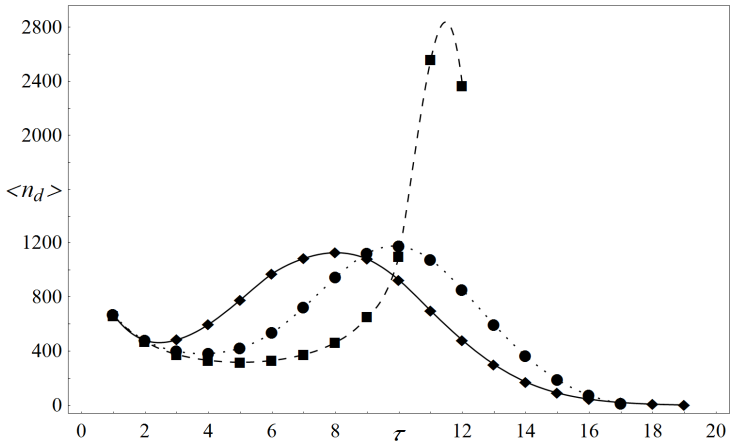

Fig. 9. Average number of damaged pillars $\langle n_d \rangle$ vs τ for hexagonal lattice. Comparison of load transfer rules: the GLS (square), the LLS (diamond) and the the VLS (circle), $N \approx 10^4$ and the averages are taken over 10^3 samples

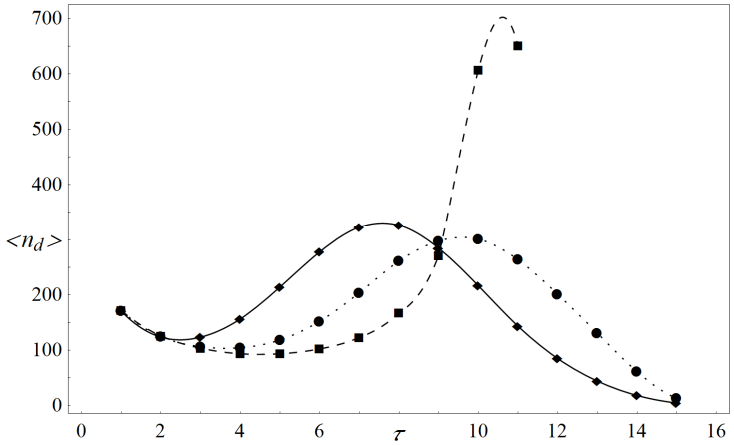

Fig. 10. Average number of damaged pillars $\langle n_d \rangle$ vs τ for triangular lattice. Comparison of load transfer rules: GLS (square), LLS (diamond) and VLS (circle), $N \approx 2.5 \times 10^3$ and the averages are taken over 10^3 samples

Our second quantity of interest, $\langle n_i(\tau) \rangle$ is computed for the population of 10^3 arrays of 10^4 pillars and thus it gives the results for the ample variety of Voronoi regions. This quantity measures the typical number of pillars which share the load

carried by one, previously destroyed pillar. In Figure 11 it has been shown comparison of number of intact elements $\langle n_i(\tau)\rangle$ per Voronoi region for different lattice types. However, the evolution of $\langle n_i(\tau)\rangle$ is similar for these lattices, there is a noticeable distinction. Especially in the early stages, the value of $\langle n_i(\tau)\rangle$ is ordered according to the values of z, namely it is highest for triangular lattice $(z=6)$ and lowest for hexagonal lattice $(z=3)$.

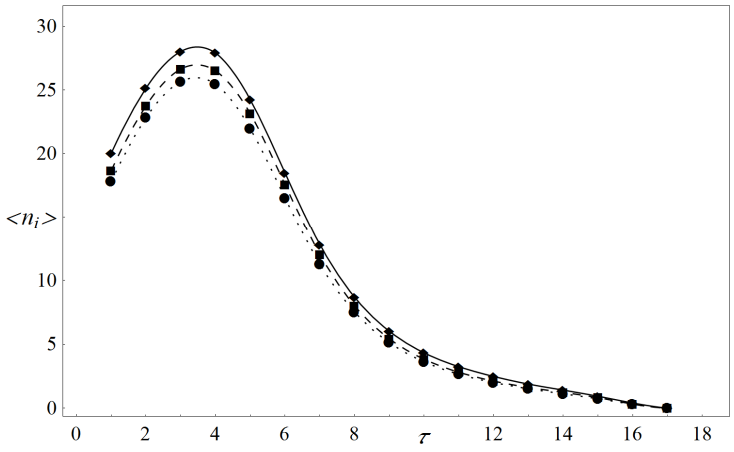

Fig. 11. Average number of intact elements $\langle n_i\rangle$ per Voronoi region vs τ with the VLS rule. Comparison of lattices: hexagonal (circle), square (square), triangular (diamond), $N \approx 10^4$ and the averages are taken over 10^3 samples

Conclusions

Numerous works have been done on the FBM generalisation. Apart from the previously mentioned two extreme approaches, the GLS and the LLS, there are also mixtures of them and models with long-range load transfer rule [16]. Besides the FBM, other approaches were used to study the fracture evolution in solids mechanics [17, 18]. Especially the models with a variable range of interactions.

Depending on the stage of load exposure the damage evolution according to the VLS rule behaves like the GLS (early stage) or the LLS (later stage) rules. It is worth to mention that the Voronoi volumes vary in time and so the VLS is range-variable rule.

In the present work, the regular tessellations and different load transfer rules have been exploited to analyse the damage evolution of the family of nanopillars. Even though the pillars are mechanically independent their arrangements can induce a kind of correlated-damage-evolution, especially seen in the framework of the VLS rule.

References

[1] Herrmann H.J., Rux S. (eds.), Statistical Models for the Fracture of Disordered Media, North Holland, Amsterdam, 1990, and references therein.

[2] Alava M.J., Nukala P.K.V.V., Zapperi S., Statistical models of fracture, Advances in Physics 2006, 55, 349-476.

[3] Moreno Y., Gomez J.B., Pacheco A.F., Fracture and second-order phase transitions, Phys. Rev. Letters 2000, 85, 2865-2868.

[4] Gomez J.B., Moreno Y., Pacheco A.F., Probabilistic approach to time-dependent load-transfer models of fracture, Phys. Rev. E 1998, 58, 1528-1532.

[5] Pradhan S., Hemmer P.C., Breaking rate minimum predicts the collapse point of over-loaded materials, Phys. Rev. E 2009, 79, 41148-41152.

[6] Okabe A., Boots B., Sugihara K., Spatial Tessellations: Concepts and Applications of Voronoi Diagrams, John Wiley & Sons, England, 1992.

[7] Weijgaert R., Vegter G., Icke V., Ritzerveld J. (eds.), Tessellations in the Sciences: Virtues, Techniques and Applications of Geometric Tailings, 2010, Springer-Verlag in press.

[8] Domański Z., Derda T., Voronoi tessellation description of load transfer within the fibres bundle model of two dimensional damage, XV-ICMFM Abstracts, 2010, 22.

[9] Domański Z., Derda T., Voronoi tessellation description of fatigue load transfer within the fibre bundle model of two dimensional damage - accepted for publication.

[10] Greer J.R., Jang D., Kim J.-Y., Burek M.J., Emergence of new mechanical functionality in materials via size reduction, Adv. Functional Materials 2009, 19, 2880-6.

[11] Burek M.J., Greer J.R., Fabrication and Microstructure Control of Nanoscale Mechanical Testing Specimens via Electron Beam Lithography and Electroplating, Nano Letters 2009, 10, 69--76.

[12] Brinckmann S., Kim J.-Y., Greer J.R., Fundamental differences in mechanical behaviour between two types of crystals at the nanoscale, Phys. Rev. Letters 2008, 100, 155502.

[13] Jang D., Greer J.R., Transition from a strong-yet-brittle to a stronger-and-ductile state by size reduction of metallic glasses, Nature Materials 2010, 9, 215-219.

[14] El-Nashar H.F., Cerdeira H.A., Dynamic scaling in ballistic deposition model for a binary system, Physical Review E 2000, 61, 6149-6155.

[15] Manal P.K., Jana D., Non-universal finite size scaling of rough surfaces, J. Phys. A: Math. Theoretical 2009, 42, 485004.

[16] Hidalgo R.C., Moreno Y., Kun F., Herrmann H.J., Fracture model with variable range of interaction, Phys. Rev E 2002, 65, 46148.

[17] Chrzanowski M., Nowak K., Cellular automata in damage mechanics: creep rupture case, Archives of Mechanics 2007, 59, 329-339.

[18] Bolander J.E., Sukumar N., Irregular lattice model for quasistatic crack propagation, Phys. Rev. B 2009, 71, 94106.